



# Interface Engineering of Si Hybrid Nanostructures for Chemical and Biological Sensing

Jinghua Li and John A. Rogers\*

Opportunities for quantitative, real-time monitoring of gases, ions, and biomolecules in the environment and in the human body motivate programs of fundamental and applied research on chemically selective sensors with fast response times. In this context, silicon field-effect transistors are of considerable interest as label-free, scalable platforms for detecting a variety of chemical and biological species. Herein, recent progress and research directions in this area are reviewed. The focus of this article is on operational parameters, device architectures, schemes for surface chemical functionalization, and methods for bio-integration across a variety of use cases. The content includes strategies that combine Si with other functional materials to create hybrid structures for enhanced sensing performance. The final section highlights some remaining challenges and provides perspectives on the future of basic research and engineering development in this field.

## 1. Introduction

Increasing needs for sensitive detection and quantitative analysis of chemical and biological species in biomedical research, preventive healthcare, clinical medicine, food safety, environmental monitoring, pollution tracking and homeland security, particularly in the broader context of visions for the Internet of Things, create significant interest in this rapidly developing area of technology. Among various engineering options,

potentiometric sensors based on field-effect transistors (FETs) are particularly promising.<sup>[1]</sup> By exploiting a three-terminal configuration to control the conductance and flow of current through a semiconductor channel, FET sensors naturally incorporate signal amplification via current modulation induced by electric fields that follow from the presence of chemical analytes, such as gaseous molecules, ions, proteins, and nucleic acids onto or adjacent to the active regions of the devices. By comparison to passive resistive or capacitive chemical sensors, such FET platforms offer significant advantages in size, power consumption, and sensitivity, in a manner that benefits strongly from alignment with materials

and processes used in the electronics industry.<sup>[2]</sup>

These and other attractive features create growing interest in this form of technology, including fundamental aspects of materials science and chemistry approaches for control over interfacial properties. Recent progress in nanomaterials synthesis methods and nanofabrication techniques create opportunities for chemical sensors with exceptionally high interfacial areas and extremely small dimensions, for enhanced performance in sensitivity and response time, respectively. Previous reports describe unique classes of sensors that exploit various types of nanomaterials and device architectures for targeted applications, with active materials that include organic semiconductors,<sup>[3,4]</sup> inorganic thin-films and nanowires,<sup>[5–9]</sup> carbon nanotubes,<sup>[10]</sup> graphene,<sup>[11]</sup> and transition metal dichalcogenides.<sup>[12]</sup> Among the broad range of investigated materials, monocrystalline Si and its derivatives are of particular interest due to excellent, reproducible, and well-controlled electronic properties, leading to superior performance and power efficient operation and offering compatibility with complementary metal-oxide-semiconductor (CMOS) technologies for integrated multiplexing and signal processing.

Various studies demonstrate the use of such classes of chemical sensing platforms with emphasis on preparation, assembly, interface engineering, electrical performance, and applications. Compared to other nanomaterials (e.g., graphene, transition metal dichalcogenides, black phosphorus) that often include a range of uncontrolled active sites (e.g., vacancies, grain boundaries and defects) with adverse effects on sensing on the basal plane, modern methods allow monocrystalline Si to be formed routinely and with exceptional quality, at low cost over large areas, with nearly perfect structural and materials characteristics.<sup>[13]</sup> Controlled growth and/or lithographic

Dr. J. Li

Department of Materials Science and Engineering  
Center for Chronic Brain Injury  
The Ohio State University  
Columbus, OH 43210, USA

Prof. J. A. Rogers

Center for Bio-Integrated Electronics  
Simpson Querrey Institute for BioNanotechnology  
Department of Materials Science and Engineering  
Biomedical Engineering  
Chemistry, Mechanical Engineering, Electrical Engineering and  
Computer Science, and Neurological Surgery  
McCormick School of Engineering and Feinberg School of Medicine  
Northwestern University  
Evanston, IL 60208, USA  
E-mail: jrogers@northwestern.edu

Prof. J. A. Rogers

Department of Materials Science and Engineering  
Frederick Seitz Materials Research Laboratory  
University of Illinois at Urbana-Champaign  
Urbana, IL 61801, USA

 The ORCID identification number(s) for the author(s) of this article can be found under <https://doi.org/10.1002/admt.202000380>.

DOI: 10.1002/admt.202000380

processing can yield nanostructured elements of silicon for improved performance in sensing devices. Surface chemical and/or functional materials modifications to the surfaces of such structures yield hybrid systems that enable specific interactions with analytes for selective chemical sensing. The result enhances capabilities and supports targeted selectivity to species of interest, with ability to support requirements for applications that lie outside of the scope of those that can be addressed with silicon alone.

This progress report article highlights recent advances in the development of these types of FET sensors, where monocrystalline Si in various forms and device architectures serves as the basis for hybrid materials combinations and heterogeneously integrated systems. The content begins with an overview of the basic operational principles, and recent advances in materials preparation, structural designs, and interface engineering strategies for Si-based FET sensors of various chemical and biological species, including gases, ions, and biomolecules, with emphasis on improving two of the most important performance metrics: sensitivity and selectivity. A following section describes concepts for fabricating such sensors, including in forms that offer capabilities beyond those supported by conventional CMOS platforms, with a focus on bio-integration, biotoxicity, and biocompatibility at the biotic/abiotic interface for wearable, skin-interfaced, and implantable devices. Representative examples highlight recent progress in scaled integration of arrays



**John A. Rogers** obtained B.A. and B.S. degrees in chemistry and in physics from the University of Texas, Austin, in 1989. From MIT, he received S.M. degrees in physics and in chemistry in 1992 and a Ph.D. in physical chemistry in 1995. After five years at Bell Laboratories, he spent thirteen years on the faculty at University of Illinois. In 2016, he joined Northwestern University as the Louis Simpson and Kimberly Querrey Professor of Materials Science and Engineering, Biomedical Engineering and Medicine, with affiliated appointments in Mechanical Engineering, Electrical and Computer Engineering, and Chemistry. Prof. Rogers also serves as Director of the Querrey–Simpson Institute for Bioelectronics.

of such sensors for large area and/or multiplexed chemical or biological sensing using top down fabrication approaches. A final section summarizes remaining challenges and opportunities for research in this field, with some perspectives on future developments.

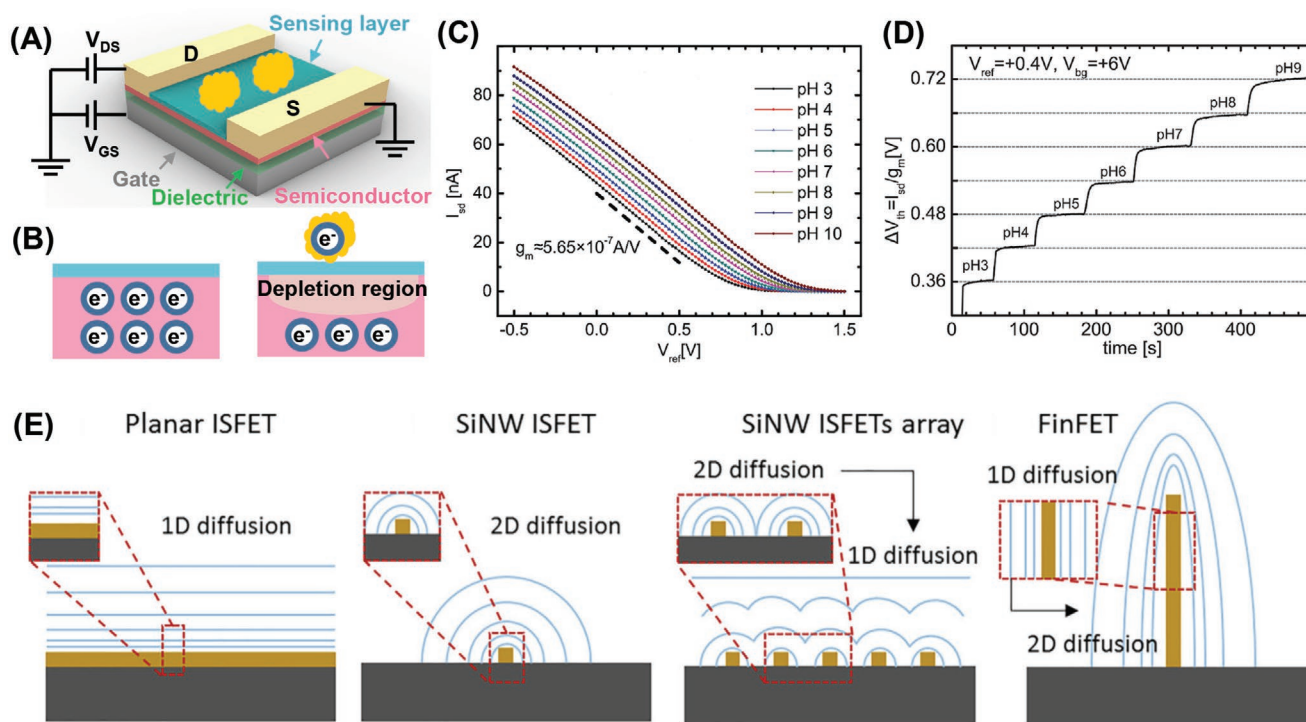


**Figure 1.** Brief overview of the fundamental operation principles of FET sensors. A) Schematic illustration of a FET chemical sensor highlighting key functional layers. B) Schematic illustration showing the change in charge carrier concentration and the generation of a depletion region in a semiconductor channel before and after the adsorption of a charged molecule. C,D) Transfer curves of a *p*-type FET pH sensor showing the shift of threshold voltage in the linear response regime C), and response to pH change as a function of time. D) Reproduced with permission.<sup>[20]</sup> Copyright 2012, American Chemical Society. E) Schematic illustration of the iso-concentration diffusion lines around the surfaces of Si-based sensors with different channel structures, highlighting the advantage of miniaturizing the geometry to improve the sensitivity and response time. Reproduced with permission.<sup>[41]</sup> Copyright 2019, Springer Nature.

## 2. Sensing Mechanisms

Although the fundamental operating principles of FET sensors are reviewed extensively elsewhere,<sup>[14–18]</sup> we begin with a brief overview to define certain concepts and terminology. In nearly all cases, such sensors share features with the conventional metal-oxide-semiconductor FET (MOSFET), a three-terminal structure that includes a semiconductor channel layer that connects the source and drain electrode, and a dielectric layer that separates this channel from the gate electrode (Figure 1A). A voltage applied between the drain to source electrodes ( $V_{DS}$ ) can drive the flow of charge carriers ( $n$ -type FET: electrons,  $p$ -type FET: holes) across the channel to produce an associated electrical current ( $I_{DS}$ ). By grounding the source and adding a voltage to the gate ( $V_{GS}$ ), charge carriers can accumulate at the interface of the semiconductor and dielectric(s), in a manner that can modulate the magnitude of  $I_{DS}$  for a given  $V_{DS}$ . By controlling the amplitude and sign of  $V_{GS}$ , the electric field can create an insulating region in the channel (known as “depletion region”) by forcing away free charge carriers, thereby switching the transistor from an “on” to “off” state (Figure 1B). The following equation describes the drain current in the regime of small  $V_{DS}$ :

$$I_{DS} = \mu C_{ox} \frac{w}{L} (V_{GS} - V_t) V_{DS} \quad (1)$$

where  $\mu$  is the mobility of the charge carriers,  $C_{ox}$  is the capacitance of the dielectric layer(s),  $w$  and  $L$  are the width and length of the channel, respectively, and  $V_t$  is known as the threshold voltage.<sup>[19]</sup> The threshold voltage corresponds to the gate voltage at which a conductive pathway forms between the source and drain. Other important characteristics of a FET, including the subthreshold swing, on/off ratio, transconductance, and hysteresis, lie outside of the scope of the present discussion. Typical semiconductors in FETs include Si (i.e., amorphous, poly, and monocrystalline Si), compound semiconductors (i.e., GaAs, InP), metal oxides (e.g., ZnO, In<sub>2</sub>O<sub>3</sub>, SnO<sub>2</sub>), organic small molecules and polymers (e.g., polycyclic aromatic hydrocarbons, perylene bisimides, poly(3-hexylthiophene)), and low dimensional materials (e.g., carbon nanotubes, graphene, MoS<sub>2</sub>, black phosphorus).

The dependence of the conductance of the semiconductor channel on the gate voltage serves as the basic working principle for FET sensors. Briefly, the binding of target ions/molecules to the surface of FETs, either directly at the channel region or at a part of the gate electrode that extends laterally from the channel can modulate the charge carrier density, in a way that is analogous to the external application of a voltage to the gate, thereby changing the conductance of the channel. This analyte-induced voltage bias on the channel causes an equivalent shift in the threshold voltage. As a result, FET sensors typically operate on the basis of measurements of either  $\Delta V_t$  or  $\Delta I_{DS}$  (Figure 1C,D).<sup>[20]</sup> The normalized current response ( $\Delta I_{DS}/I_{DS}$ ) defines the sensitivity ( $S$ ), and  $\Delta V_t$  provides direct information on the change in the surface potential at the channel caused by the adsorption of chemical and biological analytes. For the detection of biological signals in solutions,

a reference electrode usually replaces the gate electrode. The following equation describes  $V_t$ :

$$V_t = E_{ref} - \psi + \chi^{sol} - \frac{\Phi_s}{q} - \frac{Q_t}{C_{ox}} + 2\Phi_f \quad (2)$$

where  $E_{ref}$  is the reference electrode potential,  $\psi$  is the surface potential developed at the electrolyte-sensor interface,  $\chi^{sol}$  is the surface dipole potential of the solvent,  $\Phi_s$  is the work function of the semiconductor channel,  $q$  is the elementary charge,  $Q_t$  is the combination of depletion layer charges in the semiconductor, accumulated charges in the dielectric(s), and interface trap charges, and  $\Phi_f$  is the Fermi potential of the semiconductor. This governing equation serves as an effective mechanism for connecting a measurement of  $V_t$  to changes in surface potential caused by the adsorption of biomolecules.

While the majority of chemical sensing applications with FETs involve electrostatic effects associated with adsorption of analytes, in some cases, the analytes also induce changes in the work function of the metal electrodes, which then modifies the Schottky barrier between the metal and semiconductor.<sup>[21]</sup> Although this effect can frustrate quantitative interpretation of measurements with systems that do not include appropriate passivation on the metal contacts,<sup>[22]</sup> recent studies demonstrate means to leverage this physics in gas sensors that involve FET channels decorated with metal nanoparticles.<sup>[23,24]</sup> Details and discussions appear in the following section.

## 3. Structural Control

Methods for forming Si structures for FET sensors can be classified into two categories: bottom-up and top-down approaches. The first typically uses Si nanowires (NWs) prepared by vapor-liquid-solid (VLS) schemes, where metal nanoparticles serve as catalysts and deposition/assembly occurs on a substrate of interest during or after growth.<sup>[9]</sup> This method produces high-quality Si NWs with low defect densities and smooth sidewalls for transducing chemical signals. The high surface area-to-volume ratios of Si NWs support excellent sensitivity, as well as reduced detection times associated with the analyte diffusion kinetics.<sup>[25,26]</sup> Challenges for such bottom-up synthetic methods are largely in strategies for purification, integration, and manipulation that support sufficient engineering control, manufacturing throughput, and cost-effective operation. Although previous studies describe the assembly of Si NWs on substrates using fluidics<sup>[27–31]</sup> or electric fields<sup>[32–34]</sup>, and shear-mode printing,<sup>[31,35,36]</sup> control over the size and the placement of Si NWs across large areas for mass production requires further attention.

An attractive alternative exploits top-down fabrication of FETs based on NW/nanoribbon (NR) sensors that use Si nanomembranes (NMs) created from silicon-on-insulator (SOI) substrates<sup>[24,37]</sup> or bulk wafers<sup>[38–40]</sup> following advanced semiconductor process flows (i.e., lithography, deposition, etching). Deterministic control of the Si NMs/NRs/NWs formed in this way allows for size reductions and increased surface area-to-volume ratios, across a wide range, for performance that can be precisely and reproducibly matched to application requirements.

Figure 1E shows a schematic illustration of the iso-concentration diffusion lines around the surfaces of different types of Si structures, highlighting the importance of miniaturizing the geometry to improve the sensitivity.<sup>[41]</sup> While planar Si NMs respond to diffusion in one dimension, Si NWs can interact with analytes in two perpendicular dimensions to lower the detection limit and reduce the settling time compared to the planar counterparts, as expected based on reaction-diffusion theory.<sup>[42]</sup> Patterned arrays of Si NWs/NRs interact with analytes in a manner similar to that of a single NW/NR at high analyte concentrations, where analytes bind to the sensing interface within a short diffusion distance and reach equilibrium within a short time. The behavior evolves to that of a Si NM as the concentration decreases, as indicated by the equal concentration lines in Figure 1E. This effect, sometimes referred to as “dimensionally frustrated diffusion,” describes the time-dependent adsorption kinetics of fractal surfaces.<sup>[43]</sup>

Enhancing the height-to-width ratio can yield a structure, sometimes referred to as a FinFET, that enables double-sided interactions with analytes, thereby enhancing the gating effects of fields associated with adsorption events. A recent study demonstrates a FinFET (length: 14  $\mu\text{m}$ , top width: 150, 170, and 190 nm, thickness: 2.16  $\mu\text{m}$ ) with thermally grown  $\text{SiO}_2$  as a dielectric surface (thickness: 20 nm) for electrochemical sensing.<sup>[44]</sup> With a ratio of height-to-width of at least 10, this geometry supports a large total surface area, corresponding to more than twice that of otherwise similar planar structures, as discussed in Figure 1E. Such types of FinFETs with aspect ratios (height: width) of 13 exhibit  $\approx$ ten times higher conductivity compared to that with an aspect ratio of 1. In addition to providing double-sided gating capability, this device geometry increases the total surface area as well as the output current, both of which improve the signal to noise ratio (SNR). Here a higher SNR suggests that the instability associated with the environment (e.g. electrolyte fluctuations) can have reduced impact on the sensor response to changes in analyte concentrations. A complementary strategy to enhance the sensitivity relies on ultrathin Si channels that can be fully depleted of charge carriers upon chemical exposure for highly sensitive and low-power operation.<sup>[23,24,45,46]</sup>

#### 4. Gas Sensing

Additional materials can be combined with the silicon to produce hybrid structures with enhanced capabilities in sensing. Figure 2A shows a schematic illustration of a selective and low-power platform that relies on ultrathin Si NRs (length: 250  $\mu\text{m}$ , width: 5  $\mu\text{m}$ , thickness: 3.5 nm) with  $\text{SiO}_2$  dielectric surfaces (thickness: 2.5 nm) appropriately functionalized to sense certain types of gases.<sup>[24]</sup> The Si NMs used to form these Si NRs result from processing of an SOI substrate (initial top Si thickness: 70 nm) using a three-step dry (5 min)-wet (13:45 min)-dry (5 min) oxidation scheme (1000  $^\circ\text{C}$ ) followed by removal of the resulting  $\text{SiO}_2$  by immersion in a dilute solution of hydrofluoric acid. A combination of electron-beam and thermal evaporation at very slow rates ( $\approx 0.1$  to  $0.2 \text{ \AA s}^{-1}$ ) forms metal nanoparticles (Pd–Au, Ni–Pd, or Ni) with sub-5 nm diameters on the layer of native  $\text{SiO}_2$  (2.5 nm) on the Si NRs. These nanoparticles serve as selective sensing interfaces for target gases ( $\text{H}_2\text{S}$ ,  $\text{H}_2$ , and

$\text{NO}_2$ , respectively). The ultrathin metal layers that initially form from this deposition process tend to aggregate into isolated particles on the  $\text{SiO}_2$  surface even without further annealing steps due to the high surface energy of the metals compared to that of  $\text{SiO}_2$ .<sup>[47]</sup>

Adsorption of gases on the metal nanoparticles changes their work functions and, as a result, modifies the band alignment across the metal and silicon (Figure 2B). The associated changes in the threshold voltage and charge carrier density in the semiconductor lead to changes in measurable electrical parameters as a basis for sensing. Specifically, the threshold voltages decrease for reducing gases (e.g.,  $\text{H}_2\text{S}$  with Pd–Au) and increase for oxidizing gases (e.g.,  $\text{NO}_2$  with Ni). An example is in the sulfidation of Pd–Au caused by the dissociative adsorption of  $\text{H}_2\text{S}$ .<sup>[48]</sup> Here  $\text{H}_2\text{S}$  tends to decrease the work function of the metal nanoparticles by donating electrons, thereby decreasing the barrier for the injection of electrons and resulting in a decrease in the threshold voltage for *n*-type semiconductors.<sup>[21,24]</sup> A schematic illustration of band edge alignment before and after adsorption of  $\text{H}_2\text{S}$  appears in Figure 2B. In this type of device, exceptionally low detection limits (e.g.,  $\approx 1$  ppb for  $\text{H}_2\text{S}$ ) follow from the ultrathin geometry of the layer of metal nanoparticles and of the silicon channel.

The lateral dimensions of the Si NRs in this example and others can be defined reliably and precisely by electron-beam lithography, but with requirements for elaborate processing equipment. As an alternative, Figure 2C summarizes the use of polystyrene (PS) nanosphere lithography to fabricate nanomesh structures from Si NMs, subsequently decorated with Pd nanoparticles for hydrogen sensing.<sup>[49]</sup> In this method, a self-assembled monolayer of nanospheres serves as a mask for an etching step that removes the exposed Si (thickness: 60 nm) to create mesh patterns with feature sizes of 50–80 nm. Electron-beam evaporation forms a layer of Pd (thickness: 1 nm) that later aggregates into isolated nanoparticles without the need of thermal annealing, as described in the previous paragraph. Here, Schottky barriers form at the Pd/Si interfaces. When exposed to  $\text{H}_2$  gas, H atoms that dissociate from  $\text{H}_2$  molecules dissolve into the Pd, thereby converting it to  $\text{PdH}_x$  in the vicinity of the boundary to the underlying insulator layer (native oxide on Si). The  $\text{PdH}_x$  forms dipoles at the silicon interface and lowers the Schottky barrier, thereby modulating the charge carrier concentration in the semiconductor underneath.<sup>[50,51]</sup> Schematic illustrations of the formation of charge depletion regions in nanomesh sensors without and with Pd functionalization appear in Figure 2D. Figure 2E shows the results of numerically simulated electron concentrations before and after introducing a layer of Pd (work function: 5.12 eV) on the Si surface. Overall, the strategy of coupling sensing materials with Si nanostructures to create changes in band edge alignment upon chemical adsorption enables detection of a variety of gaseous analytes (e.g.  $\text{O}_2$ , NO) beyond those described here.<sup>[52]</sup>

Similar operating principles but with other forms of functionalization allow for selective detection of other gaseous chemical species for additional types of applications in healthcare and environmental monitoring. Figure 2F shows Si NW FET sensors (density:  $\approx 1$  NW per  $100 \mu\text{m}^2$ , diameter:  $40 \pm 8$  nm, length:  $8.5 \pm 1.5 \mu\text{m}$ ) with surface modifications based on molecules with nonpolar (trichloro phenethyl silane, trichloro trifluoro propyl silane, heptanoyl chloride, anthracene) and polar

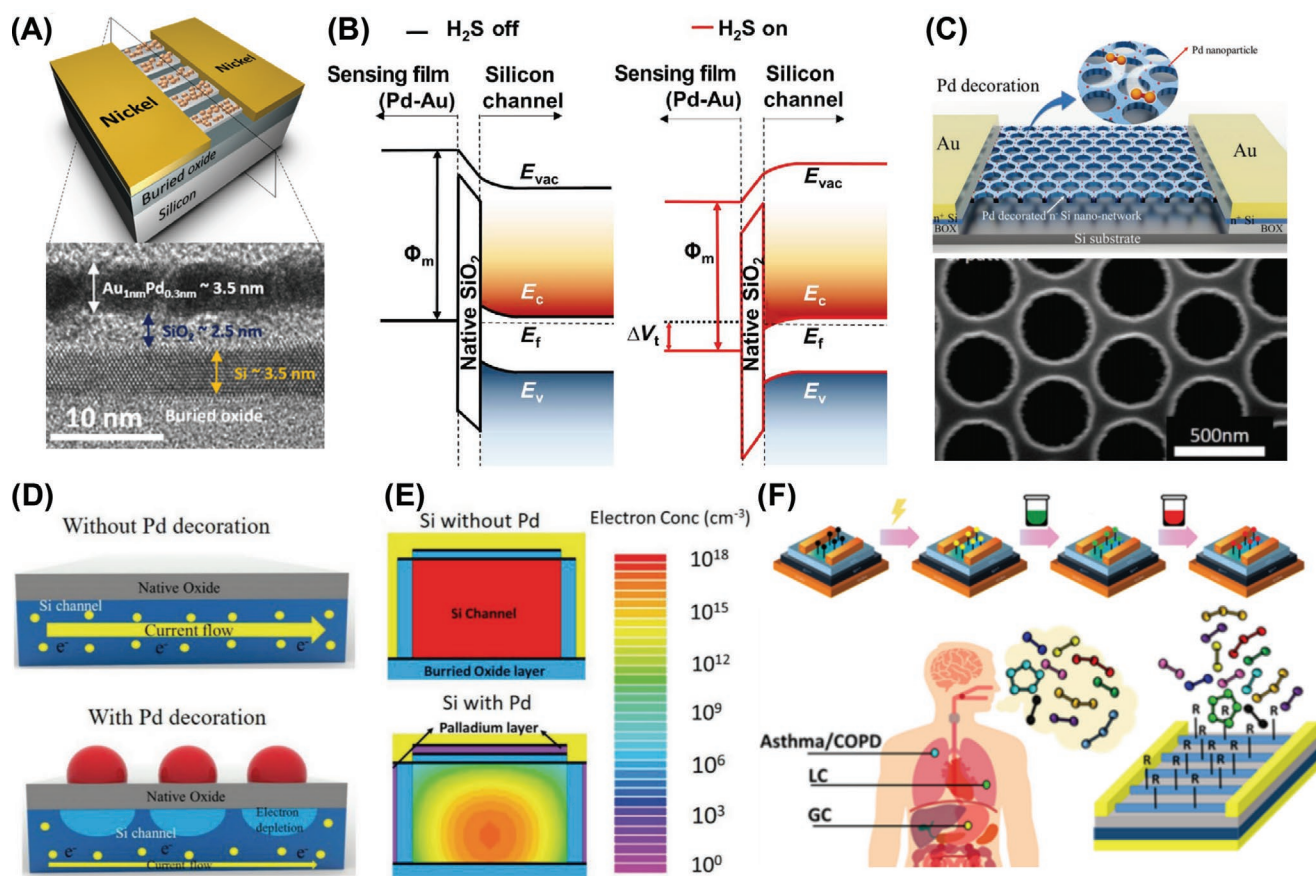


**Figure 2.** Structural engineering and surface treatment of Si-based chemical sensors for improved sensitivity and applications in gas sensing. A) Top: schematic illustration of chemically sensitive FET arrays based on ultrathin Si nanoribbons (length: 250  $\mu\text{m}$ , width: 5  $\mu\text{m}$ , thickness: 3.5 nm) with  $\text{SiO}_2$  dielectric surface (thickness: 2.5 nm) and selective sensing functionalization layers. Bottom: cross-sectional TEM image of the ultrathin Si channel. Reproduced with permission.<sup>[24]</sup> B) Schematic illustration of the band edge alignment across the Pd-Au sensing layer and Si channel before and after the exposure to  $\text{H}_2\text{S}$ . Reproduced with permission.<sup>[24]</sup> Copyright 2017, AAAS. C) Top: schematic illustration of palladium-decorated silicon nanomesh (thickness: 60 nm, diameter:  $\approx 500$  nm) fabricated by nanosphere lithography. Bottom: SEM image of Si nanomesh structure. Reproduced with permission.<sup>[49]</sup> D) Schematic illustration of the formation of depletion regions in Si nanomesh sensors without and with functionalization with Pd. <sup>[49]</sup> E) Numerically simulated electron concentration before and after formation of the Pd layer with a work function of 5.12 eV on the Si surface. Reproduced with permission.<sup>[49]</sup> Copyright 2018, Wiley-VCH. F) Schematic illustration of Si NW FET sensors (density:  $\approx 1$  NW per  $100 \mu\text{m}^2$ , diameter:  $40 \pm 8$  nm, length:  $8.5 \pm 1.5 \mu\text{m}$ ) with surface modification for the detection of volatile organic compounds (VOCs). Reproduced with permission.<sup>[53]</sup> Copyright 2016, American Chemical Society.

(APTES, bromopropyl trichlorosilane) side groups for selective detection of nonpolar and polar volatile organic compounds (VOCs), respectively.<sup>[53]</sup> These molecularly modified, cross-reactive Si NW FETs support a dynamic range between several and thousands of ppb, responding collectively to VOCs from breath samples (e.g., 2-propenenitrile, 6-methyl-5-hepten-2-one, furfural, 2-ethyl-1-hexanol, nonanal, hexane, octane). The response involves one or more of the following effects: 1) charge-charge interactions between the functional groups in the sensing layer and the VOCs, to alter the carrier density and the threshold voltage and 2) passivation of the surface states of the Si (Si-OH groups) by the VOCs, which also shifts the threshold voltage due to molecular gating<sup>[54]</sup> and affects the hysteresis behavior associated with trap states.<sup>[55]</sup> Here each type of Si NW FETs displays an assortment of independent although correlated changes (e.g., threshold voltage, charge carrier mobility and drain current) upon the exposure to one VOC with various concentrations (at ppb level). Systematic studies focus on responses

obtained with a combination of sensors with different functionalization when exposed to different VOCs. Pattern recognition methods applied to the collective output of these sensors across the various response features can, in some cases, provide sufficient information for recognizing complicated mixtures. One interesting class of application is in the development of disease breath-prints to identify lung cancer, gastric cancer, asthma, and chronic obstructive pulmonary disorders.<sup>[53,56]</sup>

## 5. pH and Ion Sensing

Surface chemical modification and functionalization can also be used in a broad range of schemes to generate specificity in sensing toward targeted ions. A collection of methods appears in **Figure 3**. The simplest example exploits the amphoteric nature of the hydroxyl groups on the surface of a native, deposited or grown layer of oxide or nitride on the surface of the Si.

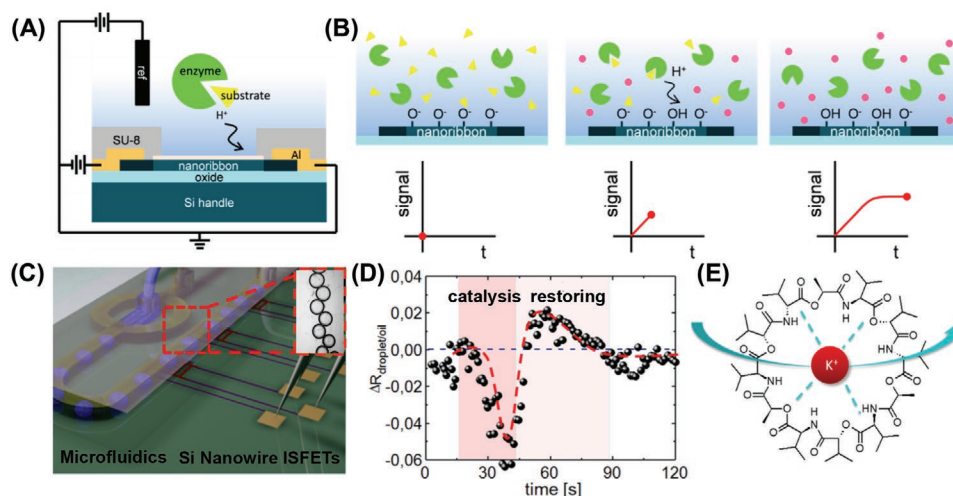


**Figure 3.** Surface treatment of Si FETs for the selective detection of pH values and ion concentrations in solution. A) Schematic illustration of Si nanoribbon devices (length: 20  $\mu\text{m}$ , width: 2  $\mu\text{m}$ , thickness: 40 nm) with  $\text{Al}_2\text{O}_3$  dielectric surfaces (thickness: 20 nm) for pH sensing to measure enzyme-substrate interactions. B) Schematic illustration of the change of signals as a function of time during the protonation of the surface oxide layer at the sensor-electrolyte interface induced by enzyme-substrate reactions. Reproduced with permission.<sup>[37]</sup> Copyright 2014, American Chemical Society. C) Schematic illustration of Si NW FET (length: 2–20  $\mu\text{m}$ , diameter: 20 nm) with  $\text{Al}_2\text{O}_3$  passivation (thickness: 20 nm) aligned with microfluidic channels for the sensing of pH and ionic strength in single solution droplets. Inset: optical image of the water-in-oil emulsions in a microfluidic channel. D) Time-dependent change of pH in droplets. The enzymatic decomposition of glucose catalyzed by GOx leads to a lowering of pH, followed by the restoring of pH in citric buffer. Reproduced with permission.<sup>[64]</sup> Copyright 2016, American Chemical Society. E) Schematic illustration showing the selective interaction between  $\text{K}^+$  and Valinomycin. Reproduced with permission.<sup>[72]</sup> Copyright 2018, American Chemical Society.

These groups switch between protonated and deprotonated states depending on the pH of a surrounding solution, thereby changing the surface charge and modulating the conductance of the channel in a Si FET, to yield a pH sensor. In an ideal situation at room temperature, the theoretical maximum sensitivity is 59.2  $\text{mV pH}^{-1}$  according to the Nernst equation (referred to as the “Nernst limit”).<sup>[57]</sup> Previous studies on Si FET pH sensors report sensitivity values typically between 30  $\text{mV pH}^{-1}$  to the Nernst limit.<sup>[20,37,58–62]</sup> Figure 3A shows Si NR devices (length: 20  $\mu\text{m}$ , width: 2  $\mu\text{m}$ , thickness: 40 nm) of this type with a layer of  $\text{Al}_2\text{O}_3$  on the silicon surface (thickness: 20 nm).<sup>[37]</sup> The schematic illustration in Figure 3B shows the dynamic change of the surface states during the protonation process at the sensor-electrolyte interface. In one application example, such sensors can quantify minute changes in pH due to proton release and/or uptake associated with the transformation of biomolecules catalyzed by enzyme solutions pipetted into the sensing reservoir (e.g., urease-urea, penicillinase-penicillin, acetylcholinesterase-acetylcholine), with a sensitivity of  $\approx 55 \text{ mV pH}^{-1}$  which is near the Nernst Limit.<sup>[63]</sup> In a specific case, urease catalyzes the hydrolysis of urea to ammonia and carbon dioxide, which then chemically converts into ammonium and bicarbonate, respectively, upon reaction with water, resulting in an increase in pH in the surrounding solution.

The ability to scale the sizes of Si-based FET sensors and to fabricate them into addressable arrays allows for high-throughput analysis of pH values and ionic strengths of single solution droplets introduced onto the sensors by integrated microfluidic structures. An example of such pH sensors based on Si NWs (length: 2–20  $\mu\text{m}$ , diameter: 20 nm,  $\text{Al}_2\text{O}_3$  dielectric surface thickness: 20 nm) appears in Figure 3C.<sup>[64]</sup> This design allows measurements of pH values and ionic strength

in single water-in-oil (e.g., dichlorobenzene) emulsion droplets. In one instance, this platform enables monitoring of enzymatic reactions for glucose detection (1 mM) by mixing the solution with glucose oxidase ( $\text{GO}_x$ ) and guiding it into a microfluidics system that interfaces to the Si FET pH sensor. Here  $\text{GO}_x$  catalyzes the oxidation of glucose to form gluconolactone, which spontaneously hydrolyzes to D-gluconic acid, resulting in the acidification of the system. Figure 3D shows the time-dependent change of pH in droplets measured by the Si NW sensor, where the enzymatic decomposition of glucose leads to transient lowering of pH in citric buffer. In addition to glucose and urea described here, the concept of utilizing enzyme-substrate reactions can apply to various important metabolites relevant to basic body functions. Overall, this type of technology can serve as an important tool for the rapid detection of on-going biochemical process (e.g., canceration,<sup>[65]</sup> embryo activity,<sup>[66]</sup> allergic responses,<sup>[67]</sup> and chondrocyte organization<sup>[68]</sup>) by sensing the interfacial pH at the cell/gate nanogap ( $\approx 50\text{--}150 \text{ nm}$ <sup>[69,70]</sup>) associated with cellular respiration. The same technology can also detect pathogens and microorganisms, and it can be used for drug screening and for establishing low-cost enrichment of nucleic acids after appropriate surface functionalization, as discussed in the following section.

In addition to pH sensing, Si FETs can serve as platforms for detecting various ions based on the interaction of cations and anions with oxide surfaces.<sup>[20,71]</sup> For enhanced specificity, ion-sensing membranes (ISM) with embedded receptors (e.g., ionophores) can be used, in devices sometimes referred to as ion sensitive FETs (ISFETs). Previous studies describe schemes for selective detection of ions with relevance to physiological and environmental conditions, such as  $\text{Na}^+$ ,  $\text{K}^+$ ,  $\text{Ca}^{2+}$ ,<sup>[72]</sup>  $\text{Hg}^{2+}$ ,  $\text{Cd}^{2+}$ ,<sup>[73]</sup>  $\text{Cu}^{2+}$ , and  $\text{Pb}^{2+}$ .<sup>[74]</sup> For example, Valinomycin (Val) is a

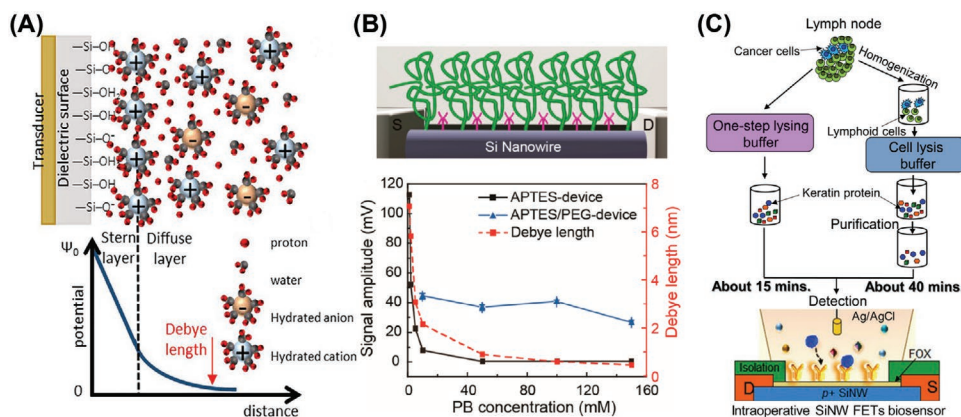


**Figure 4.** Surface functionalization of Si for the selective detection of various biological processes. A) Schematic illustration showing the formation of the Debye layer according to the Gouy-Chapman Stern model. Reproduced with permission.<sup>[41]</sup> Copyright 2019, Springer Nature. B) Top: schematic illustration of Si NW FET sensors (diameter: 30 nm) for the detection of prostate specific antigen (PSA). Bottom: dependence of the signal amplitudes for PSA sensing and the Debye length on the concentration of phosphate buffer solutions. The surface modification with polyethylene glycol (PEG) increases the effective Debye length. Reproduced with permission.<sup>[5]</sup> Copyright 2015, American Chemical Society. C) Schematic illustration of Si NW FETs (widths: 150 nm, length: 10  $\mu$ m, thicknesses: 40 nm) with SiO<sub>2</sub> dielectric surfaces (thickness: 10–15 nm) for rapid detection of disseminated tumor cells (concentration: as low as 0.01 tumor cells per mL of lymph node lysate) using keratin as the biomarker. Reproduced with permission.<sup>[95]</sup> Copyright 2016, American Chemical Society.

naturally occurring dodecadepsipeptide derived from cultures of *Streptomyces fulvissimus* for the transport of K<sup>+</sup>, and therefore can serve as the selective receptor for this ion.<sup>[75]</sup> Twelve alternating amino acids and esters form a macrocyclic molecule, where the carbonyl bonds can octahedrally coordinate with K<sup>+</sup> (radius: 1.33 Angstrom) in a square bipyramidal geometry. A schematic illustration showing the interaction between K<sup>+</sup> and Val appears in Figure 3E.<sup>[72]</sup> The radius of Na<sup>+</sup> (0.95 Angstrom) is significantly smaller than the channel, thereby preventing the formation of ionic bonds with the amino acids in Val. Similarly, the Na<sup>+</sup> ionophore X can provide high selectivity for Na<sup>+</sup> due to the formation of a cavity with appropriate dimensions for complexation with Na from calix[4]rene derivatives.<sup>[76]</sup> In another example the Ca<sup>2+</sup> ionophore IV (ETH 5234) involves diamides that show preference toward Ca<sup>2+</sup> over monovalent cations.<sup>[77]</sup> For use in sensors, the ISMs often involve plasticizers, such as polyvinyl chloride (PVC), as means to disperse the ionophores, partly to minimize potential effects of cytotoxicity.<sup>[78]</sup> Toxicity limits application of ISMs for analysis of body fluids on skin surfaces (e.g., sweat analysis).<sup>[79]</sup> The development of safe, biocompatible ISMs is important for their use in implants.

## 6. Biomolecule Sensing

A particularly compelling opportunity for silicon FET sensors is in the detection of complex biomolecules as markers of physiological processes and disease conditions. As discussed in the preceding section, Si hybrid nanostructures can support additional functionality and versatility. Functional inorganic/organic materials, for example, can provide specificity for interaction with targeted analytes. Accordingly, the choice of materials and process schemes can strongly affect the performance metrics. The most commonly used method involves the immobilization of receptors (e.g., antibodies)/enzymes on the surfaces of the Si in the channel regions through linker molecules. These organic functionalization layers can also passivate the sensor surface

and decrease the interaction with ions and nonspecific analytes. For oxide surfaces with hydroxyl groups, the most commonly applied covalent functionalization scheme relies on silane chemistry. For example, binding of (3-aminopropyl)triethoxysilane (APTES) to the surface through Si–O bonds introduces amide terminal groups for further reaction with carboxylic, aldehyde, and epoxy groups presented in proteins and other biomolecules.<sup>[80]</sup> A challenge is that nonspecific adsorption of proteins onto silanized surfaces can create background signals. Similarly, the use of other linker molecules, such as 3-mercaptopropyltrimethoxysilane(MPTMS), (3-Glycidoxypropyl)-methyl-diethoxysilane (GPTS), and (3-bromopropyl)trichlorosilane,<sup>[81–83]</sup> can also provide reactive terminal groups for the immobilization of biomolecules. For Si nanostructures without oxide dielectrics, the terminal hydrogen can react with alkenes to form surface functionalization layers.<sup>[84]</sup> In addition to covalent functionalization, approaches that exploit noncovalent interactions are also of interest due to the reversibility and capability in surface regeneration for the measurement of multiple signals.<sup>[85]</sup> For example, previous studies describe the use of coatings of biocompatible polyelectrolyte thin films grafted with oligo-ethylene-glycol. A monolayer thin film of this material attaches to the sensor surface via electrostatic forces, and the surface can regenerate by changing the pH values to frustrate such interactions.<sup>[86]</sup>

Analyte binding events lead to direct electrostatic effects that modulate the electrical characteristics of the FETs according to principles described previously. Screening of charged biomolecules by ions in the solution represents a key limitation of this sensing approach, known as Debye screening according to the Gouy-Chapman Stern model (Figure 4A).<sup>[87]</sup> Briefly, counter ions from the solution can compensate the charge of the analytes, thereby leading to an electrical potential that decreases exponentially as a function of the distance from the charged center into the surrounding solution. The distance from the sensor over which the electrostatic effect of the analytes can influence the behavior of the channel corresponds to the Debye length, typically between  $\approx 1$  and  $\approx 10$  nm, depending on the

ionic strength of the solution.<sup>[41]</sup> As a result, while the detection of relatively small analytes are straightforward, Debye screening can significantly reduce the responses for sensing of large biomolecules (e.g. proteins), where receptors (typically antibodies) can have sizes larger than the Debye length.

Figure 4B shows a strategy to enhance the effective Debye length of Si NW FET sensors (wire length: 25  $\mu\text{m}$ , diameter: 30 nm) by the addition of a mixture of polyethylene glycol (PEG) and APTES onto the Si NW surface.<sup>[5,88]</sup> This porous PEG layer, which is permeable to many biomolecules of interest, effectively increases the Debye length to facilitate the detection of biomolecules at high ionic strength. The APTES enables modification with bioreceptors needed for specificity. As an example, a Si FET functionalized with PEG can easily detect the concentration of prostate specific antigen (PSA) in phosphate buffer solution with a concentration as high as 150 nM. Here, the PEG, according to Donnan potential theory,<sup>[89]</sup> offers a nearly constant potential through its thickness due to the presence of immobilized charges, thereby increasing the effective Debye length as the Debye screening starts to occur further away from the charge center of the analyte.<sup>[89,90]</sup>

An alternative strategy focuses on the detection of byproducts of enzyme-substrate reactions, in many cases protons, in a scheme sometimes known as “enzymatic amplification.” The processes of protonation and deprotonation alter the surface potential of the channel, based on mechanisms similar to those for pH sensing, as described in the preceding session. This method serves as an electronic version of an Enzyme Linked ImmunoSorbent Assay (ELISA). Other schemes to overcome the Debye limit rely on truncated antibody receptors and small aptamers<sup>[91,92]</sup> and on methods in microfluidic pre-isolation/purification.<sup>[93]</sup> Another approach involves alternating current (AC) signals to decrease the effect of the double-layer capacitance.<sup>[94]</sup> Here, the AC electric field penetrates deeper into the solution to drive the dipoles of captured biomolecules, such that their influence can affect the transport characteristics of the channel, to generate a conductance response.

Conceptually similar strategies in functionalization allow for detection of cells. Figure 4C shows a schematic illustration of an array of Si NW FETs (widths: 150 nm, length: 10  $\mu\text{m}$ , thicknesses: 40 nm) with SiO<sub>2</sub> dielectric surface coatings (thickness: 10–15 nm) configured for rapid measurements of cancer cells.<sup>[95]</sup> Here, a washing step using 1  $\times$  PBS and then 0.01  $\times$  PBS prior to measurement decreases the ionic strength and extends the Debye length from  $\approx 0.7$  to  $\approx 8$  nm, to provide controlled measurement conditions and sufficient sensitivity. The application in this case is in direct detection of circulating tumor cells in peripheral blood from colorectal cancer patients. Here, negatively charged keratin molecules serve as the biomarker, due to their increased levels of expression in tumor cells disseminated in lymph nodes, peripheral blood and bone marrow.<sup>[96]</sup> In this system, surface functionalization exploits APTES formed by vapor-phase silanization followed by reaction with glutaraldehyde and then with a monoclonal antibody against cytokeratin. The resulting sensing platforms outperform, in terms of sensitivity (0.01 tumor cells per mL of lymph node lysate) and response time (within 1 h), standard methods based on pathological examination of tissue sections and clinical gold standard based on molecular assays. Similarly, detection of other

biomolecules using FETs are possible by immobilizing the corresponding receptors. Examples include but are not limited to neurotransmitters,<sup>[97]</sup> biomarkers,<sup>[98]</sup> nucleic acids,<sup>[99]</sup> and glycoproteins.<sup>[100]</sup> Related schemes based on Si NW FETs offer some potential for use across panels of prognostic markers for intraoperative multiplexed clinical diagnostics.

While the majority of recent work focuses on planar device designs, a frontier area is in the development of platforms that can insert into the confined 3D space of single cells. Of relevance here are nanoscale 3D transistor probes that enable highly localized, intracellular actional potential recording and pH sensing with minimal invasiveness.<sup>[101,102]</sup> These 3D probes include 1) flexible 3D kinked nanowire FETs, 2) branched intracellular nanotube Si NW FETs, and 3) Si nanotube FETs. Such probes modified with phospholipid bilayers that mimic the cell membrane can enter single cells to allow robust recording. These schemes suggest the possibility for a convergence of nanoelectronics and biological systems for real-time monitoring of fundamental cellular processes.

**Table 1** summarizes the key parameters of the devices and performance characteristics for all cases outlined in Figures 2–4. In addition to Si FET chemical sensors outlined in this review, other types of Si-based sensors can capture various chemical and biological signals. An example utilizes porous Si (PSi) formed by the etching of crystalline Si with appropriate surface functionalization as the chemical interfaces. PSi is promising for chemical sensing due to its large surface areas, tunable pore sizes and morphologies for chemical adsorption, and for its compatibility with Si processing technology. The types of devices include: 1) optical sensors that rely on changes in refractive index upon analyte infiltration into the pores, 2) electrical sensors that detect changes in capacitance and conductance induced by the adsorption of various chemical compounds, and 3) electrochemical sensors that measure current responses originated from reduction-oxidation reactions of analytes in solution at a fixed potential.<sup>[103]</sup> On-going research focuses on improving the sensitivity, selectivity, long-term stability in chemical, and biological sensing, as alternative and sometimes complementary platforms to FET-based sensors.

## 7. Applications in Wearable and Implantable Systems

Recently developed concepts in materials, design, and integration of silicon nanomaterials in flexible/stretchable electronics can be adapted for use with silicon sensors, as the basis for applications in biocompatible devices that interface with soft biological tissues, beyond small collections of cells described above. **Figure 5** presents a set of examples. Figure 5A,B shows a stretchable pH sensor built using doped Si NRs (length: 500  $\mu\text{m}$ , width: 40  $\mu\text{m}$ , thickness: 300 nm) functionalized with APTES.<sup>[104]</sup> Here, the surface  $-\text{NH}_2$  and  $-\text{SiOH}$  groups undergo protonation to  $-\text{NH}_3^+$  at low pH and deprotonation to  $-\text{SiO}^-$  at high pH, respectively. Devices of this type not only offer unique mechanical characteristics for integration with systems, but they also exploit materials that can physically disappear through hydrolysis and/or bioresorption to benign end

**Table 1.** Summary of key materials, parameters, and performance characteristics of various device platforms.

Studies	Dimension [ $\mu\text{m}$ ]	Functionalization layers	Targeted analytes	Detection limit	Response time [s]
Ref. [24]	L: 250 W: 5 T: 0.0035	Pd–Au Ni–Pd Ni	$\text{H}_2\text{S}$ $\text{H}_2$ $\text{NO}_2$	1 ppb ( $\text{H}_2\text{S}$ ) 0.3% ( $\approx 3000$ ppm) ( $\text{H}_2$ ) 1 ppm ( $\text{NO}_2$ )	$t_{90}^{\text{a}}$ : 144 (1 ppb $\text{H}_2\text{S}$ ) 17 (2% $\text{H}_2$ ) 83 (100 ppm $\text{NO}_2$ )
Ref. [49]	T: 0.06	Pd	$\text{H}_2$	$< 50$ ppm	$t_{80}$ : 3.5 (0.8% $\text{H}_2$ )
Ref. [53]	D: 0.040 L: 8.5	Organic molecules	VOCs	$\approx$ several ppb	–
Ref. [37]	L: 20 W: 2 T: 0.04	$\text{Al}_2\text{O}_3$	$\text{H}^+$	$< 0.2$ mM (urea)	$\approx 10$
Ref. [64]	D: 0.02 L: 2–20	$\text{Al}_2\text{O}_3$	$\text{H}^+$	0.5 mM (glucose)	$\approx 120$
Ref. [72]	T: 0.030	Ion-sensitive membranes	$\text{Na}^+$ , $\text{K}^+$	$< 5$ mM	$\approx 30$
Ref. [5]	D: 0.03 L: 25	APTES/PEG	Prostate specific antigen	10 nM	$\approx 500$
Ref. [95]	L: 10 W: 0.15 T: 0.040	Monoclonal antibody	Cytokeratin	$\approx 80$ fM	–

<sup>a</sup>)  $t_{90}$ : time to reach 90% of the maximum response upon exposure to chemicals.

products (e.g., Si Mg, Zn, Mo and degradable elastomers).<sup>[105]</sup> Here, dissolution of Si involves a hydrolysis step,  $\text{Si} + 4\text{H}_2\text{O} \rightarrow \text{Si}(\text{OH})_4 + 2\text{H}_2$ , with kinetics and chemical equilibria that can

be affected by various factors associated with the chemistry of the surrounding aqueous environment. Figure 5C,D highlight the process for the case of monocrystalline, device-grade

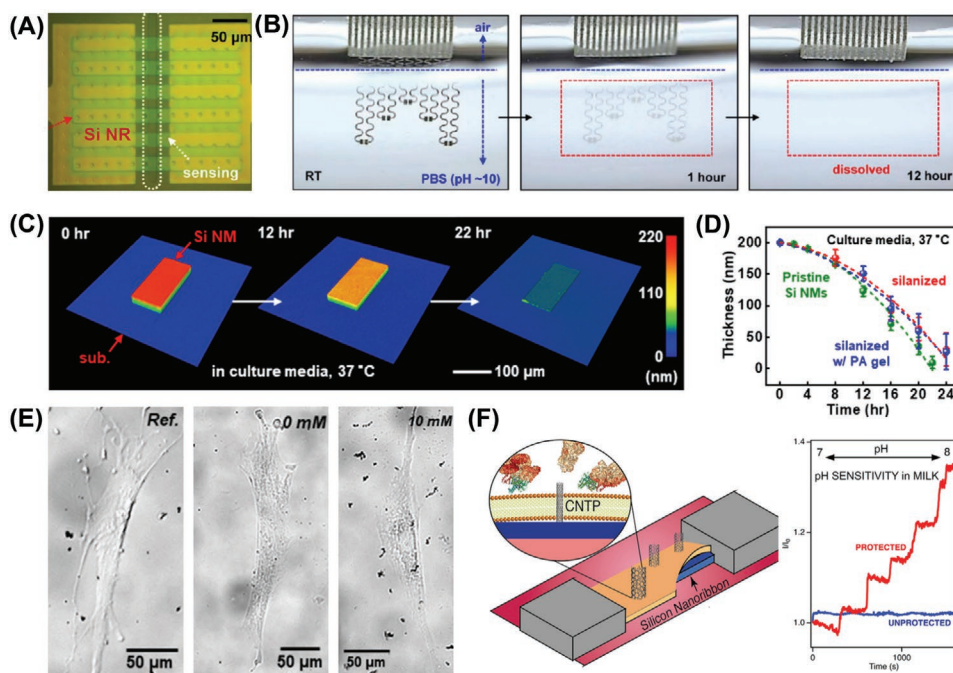


**Figure 5.** Advanced concepts for using Si NRs and NMs in bio-integrated chemical sensors. A,B) Optical microscope image of a pH sensor that uses an array of doped Si NRs (length: 500  $\mu\text{m}$ , width: 40  $\mu\text{m}$ , thickness: 300 nm) functionalized with APTES A), and photographs of a collection of bioresorbable, stretchable pH sensors based on doped Si NRs at various stages of dissolution during immersion in PBS (pH 10) at room temperature B). Reproduced with permission.<sup>[104]</sup> Copyright 2015, American Chemical Society. C) Optical profilometry images of a Si NM and line scan profiles at different stages of dissolution. D) Experimentally measured changes in thickness as a function of time for dissolution of Si NMs under various conditions. E) Optical phase-contrast images of cells under cell culture media (left), conditioned in the presence of Si NMs ( $< 1$  ppm) (middle), and after dissolution to silicic acid (10 mM) after 18 h (right). Reproduced with permission.<sup>[106]</sup> Copyright 2018, American Chemical Society. F) Schematic illustration of a Si NR FET coated with a protective lipid layer in fouling resistant pH sensors. Reproduced with permission.<sup>[107]</sup> Copyright 2019, American Chemical Society.

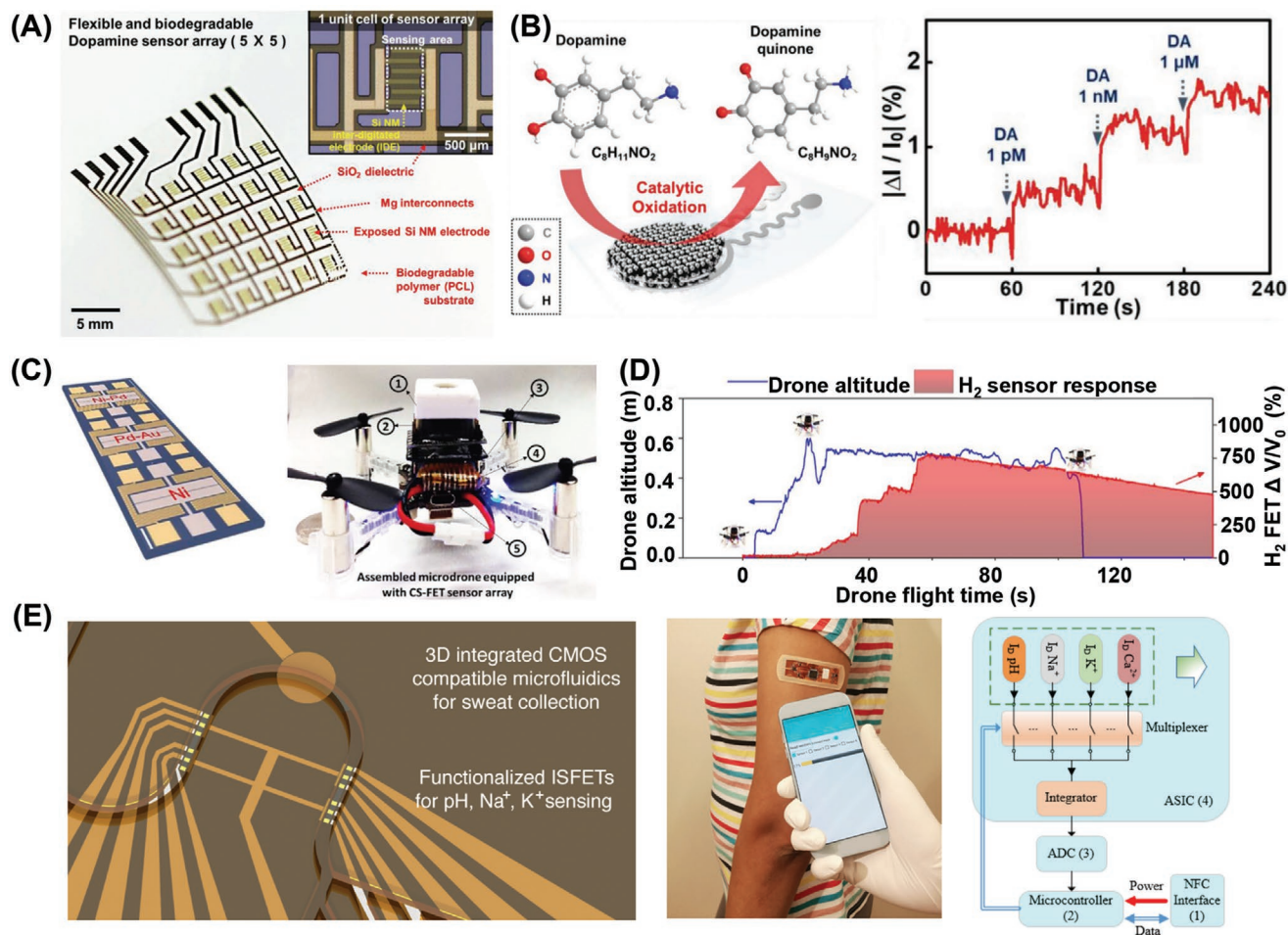


**Figure 6.** Integration of Si FETs in arrays of chemical sensors for advanced sensing applications. A) Photograph of an array (5 × 5) of flexible, bioresorbable, and passively multiplexed electrodes for spatial/temporal mapping of dopamine concentration. Inset: a Si NM-based interdigitated electrode. B) Left: schematic illustration of the sensing mechanism for dopamine at the surface of Fe<sup>3+</sup>-CPy NPs based on a modulation of the conductivity of the Si channel. Right: real-time responses of the sensor across a wide range of dopamine concentrations. Reproduced with permission.<sup>[108]</sup> Copyright 2018, Wiley-VCH. C) Left: optical image of a multifunctional chemical sensing system based on an FET array. Right: photograph showing a microdrone equipped with a sensor (right). D) Data on altitude and H<sub>2</sub> sensing response from a microdrone equipped with an H<sub>2</sub> sensor at different times during a preprogrammed flight path. Reproduced with permission.<sup>[24]</sup> Copyright 2017, AAAS. E) Left: schematic illustration of 3D ISFET sensor arrays coupled with microfluidics for sweat collection. Reproduced with permission.<sup>[72]</sup> Copyright 2018, American Chemical Society. Middle: photograph of a wireless, wearable sweat sensor for multianalyte (H<sup>+</sup>, Na<sup>+</sup>, K<sup>+</sup>, Ca<sup>2+</sup>) detection. Right: schematic illustration of the circuit for wireless communication. Reproduced with permission.<sup>[77]</sup> Copyright 2019, American Chemical Society.

Si NMs upon immersion in cell culture media.<sup>[106]</sup> The results indicate a nonlinear relationship between dissolution rate and time, suggesting possible acceleration due to the complex reaction chemistry, which could involve proteolysis, coagulation, and/or basification of proteins.<sup>[106]</sup> Figure 5E shows optical phase-contrast images of representative cells (CCD18 human colon fibroblasts) under cell culture media (left), conditioned in the presence of Si NMs (<1 ppm) (middle), and dissolved in silicic acid (10 mM) after 18 h (right). The results show high viability and normal proliferation after exposure to silicic acid, suggesting a lack of toxicity.<sup>[106]</sup>

In applications as implants, chronic immunological reactions caused by non-specific adsorption of biomolecules and cells, such as fibrotic scar formation, can isolate the devices from the surrounding environment in a manner that can compromise performance in chemical sensing. A general strategy to mitigate this issue involves separating the sensing surface

from the measurement surface of the FET. A recent study shows that Si NR FETs functionalized with an antifouling lipid bilayer containing proton-permeable carbon nanotube porin (CNTP) channels can support robust pH sensing in a variety of complex biological fluids (Figure 5F).<sup>[107]</sup> Here, carbon nanotube segments (diameter: 0.8 nm, length: ≈10 nm) insert into lipid membranes to form transmembrane channels for proton transport, while blocking most of the fouling components that arise from biological mixtures.

The rapid progress in Si-based FET sensors and the alignment of the base technology with materials and manufacturing processes used in the electronics industry facilitates translation of device concepts into practical chemical sensing platforms. **Figure 6** presents several examples of the use of scaled arrays of devices for advanced biosensing and environmental monitoring. Figure 6A shows a 5 × 5 array of flexible, and completely bioresorbable amperometric sensors.<sup>[108]</sup> Here, Si NMs functionalized

with iron-decorated carboxylated polypyrrole nanoparticles enable spatial/temporal mapping of dopamine secretion. As shown in Figure 6B, dopamine converts to dopamine-*o*-quinone in a reaction catalyzed by the nanoparticles, to generate electrons that modulate the electrical conductivity of the Si channel. This flexible and bioresorbable electrochemical system may serve as the basis for temporary implantable biochemical sensors for continuous and real-time detection of important biomarkers, such as neurotransmitters and growth factors. Functionalization with sub-5-nm metallic nanoparticles (Pd-Au, Ni-Pd, and Ni) using procedures similar to those described previously enables multiplexed gas sensing ( $\text{H}_2\text{S}$ ,  $\text{H}_2$ , and  $\text{NO}_2$ ), as shown in Figure 6C.<sup>[24]</sup> Local Joule heating elements allow for programmed recovery to baseline for repetitive use. A system level demonstration of a device of this type on a microdrone for remote  $\text{H}_2$  sensing suggests applicability in practical scenarios (Figure 6D).

Other advanced examples involve Si-based FETs co-integrated with microfluidic constructs as skin-interfaced platforms for noninvasive and real-time monitoring of biomarkers in human sweat (Figure 6E).<sup>[72]</sup> This type of system collects small volumes of sweat as it emerges from the surface of the skin and exploits capillary effects to deliver sweat to the channels of functionalized Si FET sensors for the detection of pH levels and concentrations of  $\text{Na}^+/\text{K}^+/\text{Ca}^{2+}$  separately by using different ion-sensitive membranes as described in the previous session (Figure 6E, left and middle).<sup>[72,77]</sup> Radio frequency signals power the sensors and support a readout/control interface (Figure 6E, right).<sup>[77]</sup> These same multiplexed sensor architectures can be extended to many other types of analytes through schemes for functionalizing the sensing surfaces and for limiting the effects of Debye screening, as described previously.

## 8. Perspectives

The representative results summarized here illustrate the range of applications of Si-based FET sensors for chemical and biological sensing with high sensitivity, selectivity, scalability and compatibility for bio-integration. A short review of the operating principles and primary design considerations for such devices provides context for the critical role of geometry, surface functionalization, device architecture, and integration schemes for these systems. Examples highlight sensing of various analytes in gaseous and liquid media, at the level of individual devices and complete systems. Overall, label-free sensing platforms enable detection of targeted biochemical signals without the need for tagging the molecules, and thus paves the way for rapid and inexpensive biosensing in small reaction volumes to address the needs in bio-integration and advanced healthcare.

Remaining challenges, and associated research opportunities, are in improving the two key metrics associated with any type of sensor: sensitivity and selectivity. Reducing the dimensions of semiconductor structures and devices can enhance the response associated with the electrostatics due to adsorption of analytes. On the other hand, additional crucial factors are in sources of noise and accordingly, the SNR, especially for measurements of trace amount chemicals in a complex environment. Although the underlying physics of FETs and the influence of various device parameters on noise are well

known, quantitative models of the physical chemistry aspects associated with the sensing processes themselves may help to guide strategies for optimizing the SNR through careful selection the design of materials, structures, dimensions and interfaces. Additional areas for improving capabilities for sensing of biomolecules in solution are in addressing strong screening effects that occur in biofluids, where the Debye lengths in physiological salt environments are only  $\approx 0.7$  nm.<sup>[16]</sup> In such contexts, specifically for in vivo applications, non-specific binding of species present in the complex solutions associated with blood and serum can also be difficult to eliminate.

One drawback of conventional CMOS technologies is in the requirement for relatively expensive and complicated facilities and processes. In this aspect, organic semiconductors that are intrinsically printable at low temperature in ambient environments are of interest as alternatives to Si as the building components for FET sensors. However, limitations in various key characteristics, such as long-term stability, doping control, bias stress, driving power, and signal drifting, impose significant challenges in their applications for chemical and biological sensing, especially in the context of long-term bio-integration. All such factors are important in determining materials choices and integration schemes based on specific scientific questions.

Another critical challenge for sensor technologies is in the device to device variations in performance characteristics such as threshold voltage, transconductance, on/off ratio, mobility, and hysteresis. Such variations can occur among devices from different batches or even on the same substrate. Almost all devices reviewed here possess a certain degree of variability, much of which likely arises from limited levels of materials and processing control possible in cleanroom environments available to academic research groups. For example, variations in channel thickness and doping concentration associated with thermal oxidation/diffusion processes can result in differences in response and sensitivity.<sup>[24]</sup> For the hybrid structures outlined in this article, variations can also arise from nonuniformities in surface functionalization layers and their interfaces with FET sensors. To this end, process control and quantitative calibration models are important for large-scale integration and performance improvements. The development of controllable and repeatable approaches for interface engineering also remains an interesting topic for research and requires further attention. In addition to the intrinsic properties of the sensors, environmental factors, such as humidity, can also lead to device variations. Recent studies report the integration of local on-chip microheaters to eliminate the effects of humidity to maintain the similar levels of sensitivity in changing ambient temperatures.<sup>[109]</sup>

Besides operational challenges, application in living systems demands sensors constructed in biocompatible materials, where long-term physical and chemical effects on biotissues are often unknown or poorly understood. A combination of knowledge, expertise and ideas from chemistry, materials science, electrical engineering, and biomedical engineering will be important for continued rapid progress in this important field.

This article is part of the Advanced Materials Technologies Hall of Fame article series, which recognizes the excellent contributions of leading researchers to the field of technology-related materials science.

## Conflict of Interest

The authors declare no conflict of interest.

## Keywords

bio-integrated electronics, chemical and biological sensing, field-effect transistors, interface engineering

Received: April 21, 2020

Revised: May 17, 2020

Published online: June 17, 2020

- [1] M. C. McAlpine, H. Ahmad, D. W. Wang, J. R. Heath, *Nat. Mater.* **2007**, *6*, 379.
- [2] A. Ponzoni, E. Comini, G. Sberveglieri, J. Zhou, S. Z. Deng, N. S. Xu, Y. Ding, Z. L. Wang, *Appl. Phys. Lett.* **2006**, *88*, 203101.
- [3] R. Pfattner, A. M. Foudeh, S. C. Chen, W. J. Niu, J. R. Matthews, M. Q. He, Z. N. Bao, *Adv. Electron. Mater.* **2019**, *5*, 1800381.
- [4] J. Borges-Gonzalez, C. J. Kousseff, C. B. Nielsen, *J. Mater. Chem. C* **2019**, *7*, 1111.
- [5] N. Gao, W. Zhou, X. C. Jiang, G. S. Hong, T. M. Fu, C. M. Lieber, *Nano Lett.* **2015**, *15*, 2143.
- [6] O. Knopfmacher, A. Tarasov, W. Y. Fu, M. Wipf, B. Niesen, M. Calame, C. Schonenberger, *Nano Lett.* **2010**, *10*, 2268.
- [7] C. W. Tseng, C. Y. Wen, D. C. Huang, C. H. Lai, S. Chen, Q. T. Hu, X. Chen, X. X. Xu, S. L. Zhang, Y. T. Tao, Z. Zhang, *Adv. Sci.* **2020**, *7*, 1901001.
- [8] S. Nakata, M. Shiomi, Y. Fujita, T. Arie, S. Akita, K. Takei, *Nat. Electron.* **2018**, *1*, 596.
- [9] Y. Cui, Q. Q. Wei, H. K. Park, C. M. Lieber, *Science* **2001**, *293*, 1289.
- [10] W. W. Zhou, L. Y. Mu, J. F. Li, M. Reed, P. J. Burke, *Nano Futures* **2018**, *2*, 025008.
- [11] Y. X. Liu, X. C. Dong, P. Chen, *Chem. Soc. Rev.* **2012**, *41*, 2283.
- [12] D. Sarkar, W. Liu, X. J. Xie, A. C. Anselmo, S. Mitragotri, K. Banerjee, *ACS Nano* **2014**, *8*, 3992.
- [13] S. Y. Cho, Y. Lee, H. J. Koh, H. Jung, J. S. Kim, H. W. Yoo, J. Kim, H. T. Jung, *Adv. Mater.* **2016**, *28*, 7020.
- [14] M. Kaisti, *Biosens. Bioelectron.* **2017**, *98*, 437.
- [15] Y. S. Rim, H. Chen, B. Zhu, S. H. Bae, S. Zhu, P. J. Li, I. C. Wang, Y. Yang, *Adv. Mater. Interfaces* **2017**, *4*, 1700020.
- [16] L. Mu, Y. Chang, S. D. Sawtelle, M. Wipf, X. Duan, M. A. Reed, *IEEE Access* **2015**, *3*, 287.
- [17] T. Sakata, *ACS Omega* **2019**, *4*, 11852.
- [18] J. F. Fennell Jr., S. F. Liu, J. M. Azzarelli, J. G. Weis, S. Rochat, K. A. Mirica, J. B. Ravnshæk, T. M. Swager, *Angew. Chem., Int. Ed.* **2016**, *55*, 1266.
- [19] S. M. Sze, K. K. Ng, *Physics of Semiconductor Devices*, John Wiley & Sons, New York **2006**.
- [20] A. Tarasov, M. Wipf, R. L. Stoop, K. Bedner, W. Y. Fu, V. A. Guzenko, O. Knopfmacher, M. Calame, C. Schonenberger, *ACS Nano* **2012**, *6*, 9291.
- [21] I. Heller, A. M. Janssens, J. Männik, E. D. Minot, S. G. Lemay, C. Dekker, *Nano Lett.* **2008**, *8*, 591.
- [22] B. Liu, L. Chen, G. Liu, A. N. Abbas, M. Fathi, C. Zhou, *ACS Nano* **2014**, *8*, 5304.
- [23] H. M. Fahad, N. Gupta, R. Han, S. B. Desai, A. Javey, *ACS Nano* **2018**, *12*, 2948.
- [24] H. M. Fahad, H. Shiraki, M. Amani, C. C. Zhang, V. S. Hebbbar, W. Gao, H. Ota, M. Hettick, D. Kiriya, Y. Z. Chen, Y. L. Chueh, A. Javey, *Sci. Adv.* **2017**, *3*, e1602557.
- [25] P. R. Nair, M. A. Alam, *Appl. Phys. Lett.* **2006**, *88*, 233120.
- [26] R. S. Wagner, W. C. Ellis, *Appl. Phys. Lett.* **1964**, *4*, 89.
- [27] Y. Huang, X. F. Duan, Q. Q. Wei, C. M. Lieber, *Science* **2001**, *291*, 630.
- [28] D. Whang, S. Jin, Y. Wu, C. M. Lieber, *Nano Lett.* **2003**, *3*, 1255.
- [29] S. Jin, D. M. Whang, M. C. McAlpine, R. S. Friedman, Y. Wu, C. M. Lieber, *Nano Lett.* **2004**, *4*, 915.
- [30] G. H. Yu, A. Y. Cao, C. M. Lieber, *Nat. Nanotechnol.* **2007**, *2*, 372.
- [31] Z. Y. Fan, J. C. Ho, Z. A. Jacobson, R. Yerushalmi, R. L. Alley, H. Razavi, A. Javey, *Nano Lett.* **2008**, *8*, 20.
- [32] L. F. Dong, J. Bush, V. Chirayos, R. Solanki, J. Jiao, Y. Ono, J. F. Conley, B. D. Ulrich, *Nano Lett.* **2005**, *5*, 2112.
- [33] S. Raychaudhuri, S. A. Dayeh, D. L. Wang, E. T. Yu, *Nano Lett.* **2009**, *9*, 2260.
- [34] E. M. Freer, O. Grachev, X. F. Duan, S. Martin, D. P. Stumbo, *Nat. Nanotechnol.* **2010**, *5*, 625.
- [35] R. Yerushalmi, Z. A. Jacobson, J. C. Ho, Z. Fan, A. Javey, *Appl. Phys. Lett.* **2007**, *91*, 203104.
- [36] M. Madsen, K. Takei, R. Kapadia, H. Fang, H. Ko, T. Takahashi, A. C. Ford, M. H. Lee, A. Javey, *Adv. Mater.* **2011**, *23*, 3115.
- [37] L. Y. Mu, I. A. Droujinine, N. K. Rajan, S. D. Sawtelle, M. A. Reed, *Nano Lett.* **2014**, *14*, 5315.
- [38] A. J. Baca, J. H. Ahn, Y. G. Sun, M. A. Meitl, E. Menard, H. S. Kim, W. M. Choi, D. H. Kim, Y. Huang, J. A. Rogers, *Angew. Chem., Int. Ed.* **2008**, *47*, 5524.
- [39] H. C. Ko, A. J. Baca, J. A. Rogers, *Nano Lett.* **2006**, *6*, 2318.
- [40] S. Mack, M. A. Meitl, A. J. Baca, Z. T. Zhu, J. A. Rogers, *Appl. Phys. Lett.* **2006**, *88*, 213101.
- [41] S. Rollo, D. Rani, W. Olthuis, C. P. Garcia, *Biophys. Rev.* **2019**, *1*.
- [42] P. Nair, M. Alam, *Appl. Phys. Lett.* **2006**, *88*, 233120.
- [43] P. R. Nair, M. A. Alam, *Phys. Rev. Lett.* **2007**, *99*, 256101.
- [44] S. Rollo, D. Rani, R. Leturcq, W. Olthuis, C. P. Garcia, *Nano Lett.* **2019**, *19*, 2879.
- [45] H. Jang, W. Lee, S. M. Won, S. Y. Ryu, D. Lee, J. B. Koo, S. D. Ahn, C. W. Yang, M. H. Jo, J. H. Cho, J. A. Rogers, J. H. Ahn, *Nano Lett.* **2013**, *13*, 5600.
- [46] Y. K. Choi, D. W. Ha, T. J. King, C. M. Hu, *IEEE Electron Device Lett.* **2001**, *22*, 447.
- [47] J. Nah, S. B. Kumar, H. Fang, Y.-Z. Chen, E. Plis, Y.-L. Chueh, S. Krishna, J. Guo, A. Javey, *J. Phys. Chem. C* **2012**, *116*, 9750.
- [48] C.-H. Chen, Y. H. Ma, *J. Membr. Sci.* **2010**, *362*, 535.
- [49] M. Gao, M. Cho, H. J. Han, Y. S. Jung, I. Park, *Small* **2018**, *14*, 1703691.
- [50] H. Conrad, G. Ertl, E. E. Latta, *Surf. Sci.* **1974**, *41*, 435.
- [51] M. Cho, J. Yun, D. Kwon, K. Kim, I. Park, *ACS Appl. Mater. Interfaces* **2018**, *10*, 12870.
- [52] J.-W. Han, T. Rim, C.-K. Baek, M. Meyyappan, *ACS Appl. Mater. Interfaces* **2015**, *7*, 21263.
- [53] N. Shehada, J. C. Cancilla, J. S. Torrecilla, E. S. Pariente, G. Bronstrup, S. Christiansen, D. W. Johnson, M. Leja, M. P. A. Davies, O. Liran, N. Peled, H. Haick, *ACS Nano* **2016**, *10*, 7047.
- [54] Y. Paska, T. Stelzner, O. Assad, U. Tisch, S. Christiansen, H. Haick, *ACS Nano* **2012**, *6*, 335.
- [55] Y. Paska, H. Haick, *ACS Appl. Mater. Interfaces* **2012**, *4*, 2604.
- [56] N. Shehada, G. Bronstrup, K. Funke, S. Christiansen, M. Leja, H. Haick, *Nano Lett.* **2015**, *15*, 1288.
- [57] R. Van Hal, J. C. Eijkel, P. Bergveld, *Sens. Actuators, B* **1995**, *24*, 201.
- [58] I. Park, Z. Y. Li, A. P. Pisano, R. S. Williams, *Nanotechnology* **2010**, *21*, 015501.
- [59] M. C. Chen, H. Y. Chen, C. Y. Lin, C. H. Chien, T. F. Hsieh, J. T. Horng, J. T. Qiu, C. C. Huang, C. H. Ho, F. L. Yang, *Sensors* **2012**, *12*, 3952.
- [60] S. Y. Chen, J. G. Bomer, E. T. Carlen, A. van den Berg, *Nano Lett.* **2011**, *11*, 2334.
- [61] B. R. Dorvel, B. Reddy, J. Go, C. D. Guevara, E. Salm, M. A. Alam, R. Bashir, *ACS Nano* **2012**, *6*, 6150.
- [62] J. Kwon, B. H. Lee, S. Y. Kim, J. Y. Park, H. Bae, Y. K. Choi, J. H. Ahn, *ACS Sens.* **2019**, *4*, 1724.

- [63] J. Wang, *Analytical electrochemistry Third edition*, John Wiley & Sons, Hoboken, New Jersey **2006**.
- [64] J. Schuett, B. Ibarlucea, R. Illing, F. Zoergiebel, S. Pregl, D. Nozaki, W. M. Weber, T. Mikolajick, L. Baraban, G. Cuniberti, *Nano Lett.* **2016**, *16*, 4991.
- [65] T. Sakata, H. Sugimoto, A. Saito, *Anal. Chem.* **2018**, *90*, 12731.
- [66] T. Sakata, A. Saito, J. Mizuno, H. Sugimoto, K. Noguchi, E. Kikuchi, H. Inui, *Anal. Chem.* **2013**, *85*, 6633.
- [67] H. Yang, M. Honda, A. Saito, T. Kajisa, Y. Yanase, T. Sakata, *Anal. Chem.* **2017**, *89*, 12918.
- [68] H. Satake, A. Saito, T. Sakata, *Nanoscale* **2018**, *10*, 10130.
- [69] M. C. Dos Santos, R. Déturche, C. Vézy, R. Jaffiol, *Biophys. J.* **2016**, *111*, 1316.
- [70] J. S. Burmeister, L. A. Olivier, W. M. Reichert, G. A. Truskey, *Biomaterials* **1998**, *19*, 307.
- [71] R. Sivakumarasamy, R. Hartkamp, B. Siboulet, J. F. Dufreche, K. Nishiguchi, A. Fujiwara, N. Clement, *Nat. Mater.* **2018**, *17*, 464.
- [72] E. Garcia-Cordero, F. Bellando, J. R. Zhang, F. Wildhaber, J. Longo, H. Guerin, A. M. Ionescu, *ACS Nano* **2018**, *12*, 12646.
- [73] L. B. Luo, J. S. Jie, W. F. Zhang, Z. B. He, J. X. Wang, G. D. Yuan, W. J. Zhang, L. C. M. Wu, S. T. Lee, *Appl. Phys. Lett.* **2009**, *94*, 193101.
- [74] X. Y. Bi, A. Agarwal, K. L. Yang, *Biosens. Bioelectron.* **2009**, *24*, 3248.
- [75] L. A. Pioda, V. Stankova, W. Simon, *Anal. Lett.* **1969**, *2*, 665.
- [76] P. Bühlmann, E. Pretsch, E. Bakker, *Chem. Rev.* **1998**, *98*, 1593.
- [77] J. R. Zhang, M. Rupakula, F. Bellando, E. G. Cordero, J. Longo, F. Wildhaber, G. Herment, H. Guerin, A. M. Ionescu, *ACS Sens.* **2019**, *4*, 2039.
- [78] R. Marchant, J. Anderson, E. Dillingham, *J. Biomed. Mater. Res.* **1986**, *20*, 37.
- [79] W. Gao, S. Emaminejad, H. Y. Y. Nyein, S. Challa, K. Chen, A. Peck, H. M. Fahad, H. Ota, H. Shiraki, D. Kiriya, *Nature* **2016**, *529*, 509.
- [80] F. Patolsky, G. Zheng, C. M. Lieber, *Nat. Protoc.* **2006**, *1*, 1711.
- [81] R. Ermanok, O. Assad, K. Zigelboim, B. Wang, H. Haick, *ACS Appl. Mater. Interfaces* **2013**, *5*, 11172.
- [82] B. Dorvel, B. Reddy Jr., I. Block, P. Mathias, S. E. Clare, B. Cunningham, D. E. Bergstrom, R. Bashir, *Adv. Funct. Mater.* **2010**, *20*, 87.
- [83] S.-P. Lin, T.-Y. Chi, T.-Y. Lai, M.-C. Liu, "The effect of varied functional biointerfaces on the sensitivity of silicon nanowire MOSFET", presented at **2012 IEEE-EMBS Conference on Biomedical Engineering and Sciences**, **2012**.
- [84] Y. L. Bunimovich, Y. S. Shin, W.-S. Yeo, M. Amori, G. Kwong, J. R. Heath, *J. Am. Chem. Soc.* **2006**, *128*, 16323.
- [85] X. Duan, N. K. Rajan, D. A. Routenberg, J. Huskens, M. A. Reed, *ACS Nano* **2013**, *7*, 4014.
- [86] X. Duan, L. Mu, S. D. Sawtelle, N. K. Rajan, Z. Han, Y. Wang, H. Qu, M. A. Reed, *Adv. Funct. Mater.* **2015**, *25*, 2279.
- [87] R. E. G. vanHal, J. C. T. Eijkel, P. Bergveld, *Adv. Colloid Interface Sci.* **1996**, *69*, 31.
- [88] N. Gao, T. Gao, X. Yang, X. C. Dai, W. Zhou, A. Q. Zhang, C. M. Lieber, *Proc. Natl. Acad. Sci. USA* **2016**, *113*, 14633.
- [89] H. Ohshima, *Sci. Technol. Adv. Mater.* **2009**, *10*, 063001.
- [90] N. Haustein, O. Gutierrez-Sanz, A. Tarasov, *ACS Sens.* **2019**, *4*, 874.
- [91] R. Elnathan, M. Kwiat, A. Pevzner, Y. Engel, L. Burstein, A. Khatchourints, A. Lichtenstein, R. Kantaev, F. Patolsky, *Nano Lett.* **2012**, *12*, 5245.
- [92] K. Maehashi, T. Katsura, K. Kerman, Y. Takamura, K. Matsumoto, E. Tamiya, *Anal. Chem.* **2007**, *79*, 782.
- [93] E. Stern, A. Vacic, N. K. Rajan, J. M. Criscione, J. Park, B. R. Ilic, D. J. Mooney, M. A. Reed, T. M. Fahmy, *Nat. Nanotechnol.* **2010**, *5*, 138.
- [94] C. Laborde, F. Pittino, H. A. Verhoeven, S. G. Lemay, L. Selmi, M. A. Jongsma, F. P. Widdershoven, *Nat. Nanotechnol.* **2015**, *10*, 791.
- [95] D. P. Tran, M. A. Winter, B. Wolfrum, R. Stockmann, C. T. Yang, M. Pourhassan-Moghaddam, A. Offenhausser, B. Thierry, *ACS Nano* **2016**, *10*, 2357.
- [96] V. Karantza, *Oncogene* **2011**, *30*, 127.
- [97] J. Kim, Y. S. Rim, H. Chen, H. H. Cao, N. Nakatsuka, H. L. Hinton, C. Zhao, A. M. Andrews, Y. Yang, P. S. Weiss, *ACS Nano* **2015**, *9*, 4572.
- [98] W. Huang, K. Besar, R. LeCover, P. Dulloor, J. Sinha, J. F. M. Hardigree, C. Pick, J. Swavola, A. D. Everett, J. Frechette, *Chem. Sci.* **2014**, *5*, 416.
- [99] E. Dmitrienko, O. Naumova, B. Fomin, M. Kupryushkin, A. Volkova, N. Amirkhanov, D. Semenov, I. Pyshnaya, D. Pyshnyi, *Nanomedicine* **2016**, *11*, 2073.
- [100] T. Minamiki, T. Minami, Y. Sasaki, S.-i. Wakida, R. Kurita, O. Niwa, S. Tokito, *Sensors* **2016**, *16*, 2033.
- [101] B. Tian, T. Cohen-Karni, Q. Qing, X. Duan, P. Xie, C. M. J. S. Lieber, *Science* **2010**, *329*, 830.
- [102] X. Duan, T.-M. Fu, J. Liu, C. M. Lieber, *Nano Today* **2013**, *8*, 351.
- [103] F. A. Harraz, *Sens. Actuators, B* **2014**, *202*, 897.
- [104] S. W. Hwang, C. H. Lee, H. Y. Cheng, J. W. Jeong, S. K. Kang, J. H. Kim, J. Shin, J. Yang, Z. J. Liu, G. A. Ameer, Y. G. Huang, J. A. Rogers, *Nano Lett.* **2015**, *15*, 2801.
- [105] S.-K. Kang, J. Koo, Y. K. Lee, J. A. Rogers, *Acc. Chem. Res.* **2018**, *51*, 988.
- [106] J. K. Chang, M. A. B. Emon, C. S. Li, Q. S. Yang, H. P. Chang, Z. J. Yang, C. I. Wu, M. T. Saif, J. A. Rogers, *ACS Nano* **2018**, *12*, 9721.
- [107] X. Chen, H. N. Zhang, R. H. Tunuguntla, A. Noy, *Nano Lett.* **2019**, *19*, 629.
- [108] H. S. Kim, S. M. Yang, T. M. Jang, N. Oh, H. S. Kim, S. W. Hwang, *Adv. Healthcare Mater.* **2018**, *7*, 1801071.
- [109] N. Gupta, H. M. Fahad, M. Amani, X. Song, M. Scott, A. Javey, *ACS Sens.* **2019**, *4*, 1857.